Photochemical & Photobiological Sciences (2025) 24:2153–2168
https://doi.org/10.1007/s43630-025-00820-w

RESEARCH

# Photobiomodulation therapy enhances surfactant production in premature rat lungs: a non-invasive therapeutic strategy for neonatal respiratory distress syndromes

**Halil İbrahim Özdemir[1] · Ertuğrul Özkan[5] · Metin Bilge[5] · Züleyha Özçelik Çetinel[5] · Duygu Bilge[5] · Cansın Şirin Tomruk[6] · Canberk Tomruk[6] · Hatice Elif Özdemir[2] · Ayshan Ahadova[3] · Ayşe Çekin[3] · Nur Selvi Günel[3] · Çağla Kayabaşı[4] · Demet Terek[8] · Elif Erol[9] · Fahri Emrah Soylu[10] · Şenay Şanlıer[7] · Mehmet Yalaz[8] · Cumhur Gündüz[3] · İsmail Oran[1]**

Received: 18 September 2025 / Accepted: 18 November 2025 / Published online: 1 December 2025


## Abstract

This study aimed to evaluate the effects of infrared photobiomodulation (PBM) on alveolar surfactant cells and explore cellular-level biological responses in preterm rat lungs. The development of supportive treatments for lung diseases could be advanced by understanding PBM's influence on alveolar type II cell function, surfactant production, and inflammatory responses. Sixty-eight preterm Sprague-Dawley rats were divided into three groups: a control group and two experimental groups receiving either 660 nm and 830 nm photobiomodulation therapy (PBMT) at 30 mW and 3 J/cm², administered three times daily for three days. Key physiological parameters were monitored, and surfactant proteins were quantified using ELISA. Additionally, cytotoxicity and genotoxicity were evaluated in H-6053 cells, and histological assessments were performed to identify structural changes. The results demonstrated that 660 nm PBMT significantly increased Surfactant B, C, and D levels. Crucially, this intervention showed no evidence of cytotoxic or phototoxic damage. In contrast, the 830 nm PBMT yielded more variable increases in surfactant proteins and was associated with minimal cytotoxic effects. These findings suggest that 660 nm PBMT is a promising, noninvasive modality for augmenting surfactant production. This approach holds potential as a supportive therapy for neonates with respiratory distress syndrome. Further clinical investigations are warranted to validate these findings in human preterm infants and to fully elucidate the underlying cellular mechanisms.

**Keywords** Respiratory distress syndrome (RDS) · Alveolar surfactant · Lung epitelial alveolar cells · Infrared LED/laser therapy · Premature · Photobiomodulation therapy (PBMT)

✉ Metin Bilge
metin.bilge@ege.edu.tr

[1] Faculty of Medicine Department of Radiodiagnostics, Ege University, Izmir, Turkey

[2] Faculty of Medicine Department of Norology, Manisa Celal Bayar University, Manisa, Turkey

[3] Faculty of Medicine Department of Medical Biology, Ege University, Izmir, Turkey

[4] Faculty of Medicine Department of Medical Biology, Balıkesir University, Balıkesir, Turkey

[5] Faculty of Science Department of Physics, Ege University, Izmir, Turkey

[6] Faculty of Medicine Department of Histology and Embriology, Ege University, Izmir, Turkey

[7] Faculty of Science Department of Biochemistry, Ege University, Izmir, Turkey

[8] Faculty of Medicine Department of Child Health and Diseases, Ege University, Izmir, Turkey

[9] Clinical Research Associate, IQVIA, Istanbul, Turkey

[10] EGEHAYMER, Ege University, Izmir, Turkey

## 1 Introduction

The lungs are highly specialized organs responsible for gas exchange between the external environment and the body. This process occurs in microscopic air sacs known as alveoli. The functional integrity of the alveolar surface is maintained by pulmonary surfactant, a lipoprotein complex that reduces surface tension and prevents alveolar ecollapse during both inspiration and expiration. This vital substance is primarily synthesized by type II alveolar epithelial cells, also referred to as alveolar surfactant cells [1]. Pulmonary surfactant is composed mainly of phospholipids and surfactant proteins (SP-A, SP-B, SP-C, and SP-D), and plays multifaceted roles in respiratory mechanics, immune responses, and cellular repair processes [2].

In conditions such as acute lung injury, newborn respiratory distress syndrome (RDS), acute respiratory distress syndrome (ARDS), and chronic inflammatory lung diseases, the function of alveolar type II cells is significantly impaired. This dysfunction leads to decreased surfactant production, disruption of the alveolar-capillary barrier, and alveolar collapse [3]. Targeting these pathophysiological mechanisms necessitates the development of alternative therapeutic approaches. In recent years, photobiomodulation therapy (PBMT), a non-invasive modality with the potential to enhance cellular metabolism, has emerged as a promising strategy in the treatment of lung diseases.

PBM is typically performed using low-intensity laser or light-emitting diode (LED) light within the infrared (600–1100 nm) or visible wavelength ranges. The light is absorbed by intracellular chromophores, particularly cytochrome c oxidase, leading to increased mitochondrial activity and ATP production, modulation of reactive oxygen species, and activation of anti-inflammatory and antioxidant signaling pathways. These effects collectively promote cellular proliferation, repair, and differentiation [4, 5].

Studies conducted in animal models have demonstrated that these biological effects of PBM are also valid in vivo. Specifically, experimental studies in rat models have shown that infrared PBM reduces inflammatory cytokines (TNF-α, IL-6, IL-1β), balances oxidative stress markers, and exerts histopathologically protective effects on pulmonary tissue [6, 7]. PBM also holds potential for preserving alveolar structure and regulating type II cell functions. For instance, a study by Seifert et al. (2021) demonstrated that infrared PBM attenuated lipopolysaccharide (LPS)-induced lung inflammation in a rat model and preserved the histological integrity of alveolar architecture [8].

However, studies specifically investigating the direct effects of PBM on alveolar surfactant cells remain limited. Although in vitro cell culture models have reported that PBM enhances cellular proliferation and surfactant protein expression, the extent to which these effects are replicated at the alveolar level in vivo, particularly in rat models, remains unclear [9]. Therefore, a detailed investigation into the effects of PBM on alveolar type II cell function, surfactant production, and inflammatory responses may contribute to the development of a supportive therapeutic approach for lung diseases.

This study aims to evaluate the effects of infrared photobiomodulation on alveolar surfactant cells in rat lungs and to explore the cellular-level biological responses to this application.

This study represents the first investigation in the literature examining the application of PBMT as a non-invasive method for treating respiratory distress syndrome (RDS) in premature rat pups. The PBMT device used in this study was custom-developed by our team, designed to deliver both LED and laser applications at a 660 nm wavelength. We hypothesize that this non-invasive treatment approach could serve as a valuable alternative to current invasive surfactant administration methods.

## 2 Materials and methods

### 2.1 Animal model, breeding, and preterm neonatal care

In this study, ten female Sprague-Dawley albino rats (200–240 g, 8–10 weeks old) were obtained from the Laboratory Animal Research and Application Center (EGEHAYMER) and housed individually under standardized conditions. Each cage was maintained at 24 ± 1 °C with a 12-hour light/dark cycle and contained wood shavings as bedding. Animals received a standard laboratory diet ad libitum, and cage cleaning was performed daily. A one-week acclimatization period allowed for environmental adaptation and familiarization with the researchers. To determine reproductive suitability, daily vaginal smear samples were collected, air-dried, fixed with methanol, and stained with 5% Giemsa. Smears were examined under a light microscope to identify the estrous cycle phase, and females in proestrus/estrus were selected for mating. Pregnancy was confirmed by the detection of sperm in vaginal smears or the presence of a vaginal plug.

Cesarean sections were performed on confirmed pregnant females. Preliminary attempts at delivery on gestational day 18 resulted in non-viable pups. Consequently, preterm delivery was conducted on gestational days 19–20 under inhalational isoflurane anesthesia. Immediately following cesarean section, newborns were rapidly dried, and any membranes were removed (Figure SI1). Preterm neonates were then transferred to a temperature- and

humidity-controlled neonatal incubator equipped with heating pads to support thermoregulation (Figure SI2).

To prevent maternal cannibalism, neonates were permanently separated from their mothers at the time of cesarean delivery. Specialized intensive care units were used to meet the physiological requirements of these preterm rats, with close monitoring of vital parameters. An orogastric tube was used to provide 0.1 mL of Esbilac formula (200 kcal/kg/day) every two hours for 96 h. This feeding regimen ensured adequate caloric intake and hydration, thereby improving the likelihood of survival and reducing hypoglycemic events. All animal procedures were approved by the Local Animal Experiments Ethics Committee (protocol number 2021-077, dated 29.09.2021), and all efforts were made to minimize discomfort and distress throughout the study.

## 2.2 PBMT system development, protocol, and experimental design

In this study, both LED and laser were used. LED can reach rat lungs and partially human infant lungs. However, since human skin is thicker than rat skin and the body is larger, laser use was included in the experiments to address the possibility of LED being insufficient. Additionally, considering that it may be effective in adults with respiratory failure syndrome who are intubated due to the coronavirus, the aim was to also observe the results of the laser. In this study, a comprehensive PBMT system was designed and implemented to evaluate the therapeutic effects of LED and laser light sources on preterm rat neonates. The design phase commenced with the creation of an LED screen control unit and LED/laser devices using AutoCAD software. Once the external casing was fabricated, electronic components were carefully integrated to ensure proper data and power transmission. In a second phase, specialized devices for direct application on rats were developed, employing both laser and LED light sources. All components were produced using a Creality CR-10 Smart Pro 3D printer with polylactic acid (PLA) filament, followed by assembly, adhesion, and meticulous surface finishing (Figure SI3).

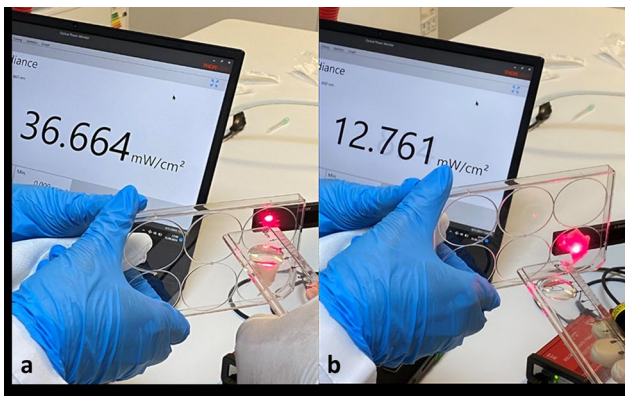


**Fig. 1** Energy absorption measurements in rat pup skin: **a** laser light permeability through plexiglass, **b** laser permeability measurements of rat pup skin stretched over plexiglass

A key element in the control architecture was the Arduino Uno microcontroller board, which received user inputs and monitored the duration of each experimental session. The microcontroller was linked to a five-inch Nextion touchscreen via a Universal Asynchronous Receiver/Transmitter (UART) communication protocol. This arrangement provided an intuitive interface for operating both laser and LED devices. Programming of the microcontroller and the touchscreen was accomplished using the Arduino IDE and Nextion Editor software, respectively. To achieve the requisite voltage and current levels for stable LED and laser operation, dedicated voltage regulation and LED driver circuits were installed. Optical power measurements were subsequently performed using a Thorlabs S130VC sensor linked to a PM100USB USB interface module, with data acquisition conducted via Thorlabs Optical Power Monitor software. Based on these measurements, precise exposure durations were calculated using the formula Joule = Watt × Second, ensuring the delivery of consistent energy irradiances.

After in vivo experiments, an in vitro experiment was conducted using human primary alveolar epithelial H-6053 cells. Results from this preliminary study indicated that exposure to 660 nm LED light increased surfactant production by 1.25-fold and enhanced cell proliferation by 25% in comparison to non-exposed controls [10]. Guided by these findings, the in vivo protocol involved the application of 660 nm LED or laser light at an energy density of 3 J/cm², three times daily for three consecutive days (72 h). However, it was recognized that rat skin exhibits significantly higher light absorption than standard cell culture conditions. It was expected that the skin of the rat pups would absorb the LED and laser beams. To determine this absorption amount, irradiance measurements were performed using the Thorlabs S130VC sensor, as shown in Fig. 1.

These measurements were first performed without placing the premature rat skin in the setup. Then, the freshly removed premature rat skin was placed in the measurement setup, and the measurement was repeated. This method determined how much irradiance from the 660 nm and 830 nm LED and laser light sources reaching the rats was absorbed by the skin (Table 1). Furthermore, since there was no obstacle that would cause absorption in the cell culture experiments, absorption did not occur. These measurements informed subsequent energy corrections and allowed for refinement of exposure durations (Fig. 1; Table 2).

A total of 68 preterm rat neonates were initially enrolled and allocated to five groups, each subjected to distinct PBMT conditions (Table 3).

**Table 1** Irradiance absorption by baby rat skin

| Wavelength (nm) | Type of light source | Irradiance before skin absorbation (mW/cm$^2$) | Irradiance after skin absorbation (mW/cm$^2$) |
|---|---|---|---|
| 660 | LED | 16.2 ± 0.11 | 8.0 ± 0.11 |
| 660 | Laser | 36.9 ± 0.1 | 12.8 ± 0.1 |
| 830 | LED | 9.2 ± 0.1 | 4.7 ± 0.1 |
| 830 | Laser | 26.5 ± 0.09 | 9.3 ± 0.09 |

Over the course of the study, 37 neonates did not survive beyond the fourth day due to various factors, leaving 31 viable subjects at study completion. PBMT sessions were administered per the established protocol, with additional focus on comparing LED and laser devices. Laser applications were included to test whether deeper tissue penetration might enhance surfactant production in neonatal lung tissue or induce cellular damage. The working hypothesis posited that, in human preterm neonates, Consequently, both 660 nm and 830 nm sources operating at 30 mW were evaluated at an energy density of 3 J/cm², delivered three times daily for three days (72 h) via LED and broad-focus infrared laser devices (Fig. 2; Table 2).

**Table 3** Our experimental groups and combinations are shown

| | | |
|---|---|---|
| Group 1 | Premature control | Day 19–20 caesarean section, premature baby rats, no mother. |
| Group 2 | Normal control | Day 22 normal birth baby rats, with mother. |
| Group 3 | 660 nm LED | Day 19–20 caesarean section, premature baby rats, no mother. |
| Group 4 | 660 nm Laser | Day 19–20 caesarean section, premature baby rats, no mother. |
| Group 5 | 830 nm LED | Day 19–20 caesarean section, premature baby rats, no mother. |
| Group 6 | 830 nm Laser | Day 19–20 caesarean section, premature baby rats, no mother. |

Table 4, which includes irradiation and PBMT parameters, was created similarly to Jenkins and Carroll's study [11]. This design enabled a direct comparison of treatment depth, potential benefits in surfactant regulation, and the risk of cellular injury under laser versus LED exposure.

## 2.3 Physiological assessments and monitoring

In this study, multiple physiological parameters were measured to evaluate the impact of PBMT on preterm

**Table 2** Shows our experimental groups, infrared PBMT energy densities, durations, and survival rates

| Condition | Wavelength (nm) | Nominal power (mW) | Irradiance (mW/cm²) | Energy density (J/cm²) | Exposure time (s) | 19–20.days (cesarean-premature) | 21–22.days (normal-mature) | Total |
|---|---|---|---|---|---|---|---|---|
| Control | – | – | 0 | 0 | 0 | 5 | 5 | 10 |
| PBMT with LED | 660 | 30 | 8.0 ± 0.11 | 3 | 375 | 6 | 0 | 6 |
| PBMT with Laser | 660 | 30 | 12.8 ± 0.1 | 3 | 234 | 5 | 0 | 5 |
| PBMT with LED | 830 | 30 | 4.7 ± 0.1 | 3 | 643 | 5 | 0 | 5 |
| PBMT with Laser | 830 | 30 | 9.3 ± 0.09 | 3 | 321 | 5 | 0 | 5 |
| Total | – | – | – | – | – | 26 | 5 | 31 |

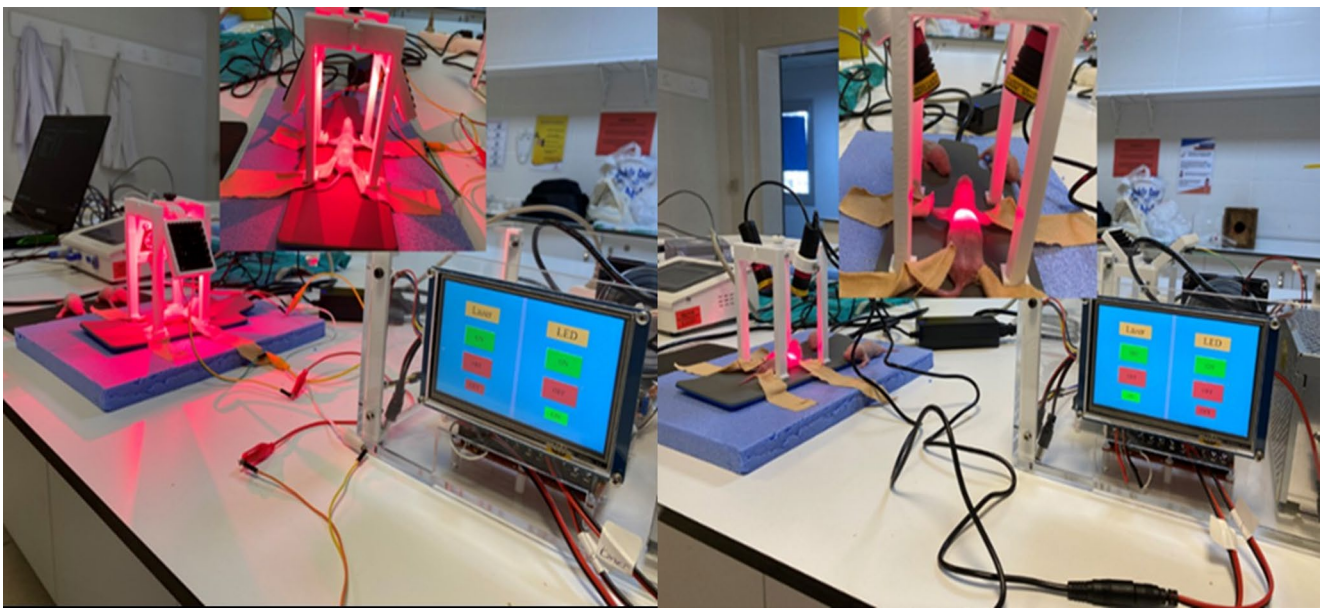

**Fig. 2** Infrared LED and broad-focus laser PBMT application on rat pups

**Table 4** Irradiation and PBMT parameters

| PBMT condition | 660 nm LED | 660 nm laser | 830 nm LED | 830 nm laser |
|---|---|---|---|---|
| Center wavelength | 660 | 660 | 830 | 830 |
| Opertaion mode | Continuous wave (CW) | Continuous wave (CW) | Continuous wave (CW) | Continuous wave (CW) |
| Average radiant power (mW) | 20.4 ± 0.11 | 32.6 ± 0.1 | 11.9 ± 0.1 | 23.7 ± 0.09 |
| Polarization | No | No | No | No |
| Beam shape | Circular | Circular | Circular | Circular |
| Beam profile | Gaussian | Gaussian | Gaussian | Gaussian |
| Irradiance at target ($mW/cm^2$) | 8.0 ± 0.11 | 12.8 ± 0.1 | 4.7 ± 0.1 | 9.3 ± 0.09 |
| Exposure duration (sec) | 375 | 234 | 643 | 321 |
| Energy density ($J/cm^2$) | 3 | 3 | 3 | 3 |
| Number of points irradiated | 2 (both lungs) | 2 (both lungs) | 2 (both lungs) | 2 (both lungs) |
| Application technique | 6 cm away from the skin surface | 6 cm away from the skin surface | 6 cm away from the skin surface | 6 cm away from the skin surface |
| Number and frequency of treatment sessions | 3 per day, total 3 days | 3 per day, total 3 days | 3 per day, total 3 days | 3 per day, total 3 days |

rat neonates. Body temperature was recorded prior to and immediately following LED and laser light applications, using a remote infrared sensor (Figure SI4a, b). This approach ensured minimal handling and reduced stress-related temperature fluctuations. Additionally, body weights, body temperatures, oxygen saturation levels, heart rates, and respiratory rates were obtained at baseline (day 0) and after the final PBMT session on day 5. Measurements of oxygen saturation and heart rate were conducted using a Covidien neonatal heart rate and lung saturation monitor ($SpO_2$), which was placed on the pelvic region (iliac and femoral arteries) to achieve the most reliable data (Figure SI4d). Respiratory rates and heart rates were also monitored using an EKG Holter sensor capable of remote measurement, ensuring continuous and accurate monitoring (Figure SI4c). Body weights were determined with a precision scale on days 0 and 5 to assess growth trajectories and any potential impact of PBMT on weight gain. These measurements offered insights into physiological stability while identifying potential adverse effects related to PBMT. These physiological assessments allowed for the evaluation of safety and efficacy in the application of LED and laser PBMT methods.

## 2.4 Surfactant analysis in premature rat lungs

In order to evaluate changes in surfactant production following LED and laser light exposure, lung lavage fluid was collected from preterm pups and prepared for surfactant protein analysis. The fluid was initially centrifuged at 5,000 rpm for 10 min. Surfactant Protein A, B, C, and D levels were then measured using Rat Surfactant Protein ELISA Kits (Novus Biologicals), strictly following the manufacturer's instructions. Standards and appropriately diluted samples (100 µl each) were pipetted into a 96-well microplate and incubated at 37 °C for 120 min. Subsequently, a biotinylated detection antibody solution was added, followed by another 60-minute incubation at the same temperature. After performing the recommended washing steps, an avidin-conjugated horseradish peroxidase (HRP) solution was introduced, and the plate was incubated for an additional hour at 37 °C. Multiple wash cycles were then carried out to remove unbound components. The substrate reagent was added and allowed to react for 15 to 30 min under dark conditions at 37 °C. Finally, the enzymatic reaction was halted using a stop solution, and optical density was recorded at 450 nm using a Thermo Multiskan FC microplate reader. This protocol provided consistent and reliable quantification of surfactant proteins in preterm rat lung tissue.

## 2.5 In vitro phototoxicity and cellular response analyses

To investigate the potential adverse effects of PBMT, an in vitro study was conducted using human lung type 2 alveolar epithelial cells (H-6053, Cell Biologics, Chicago, USA) after in vivo studies. These cells were exposed to PBM therapy at optimal, suboptimal, and supramaximal energy density, and three complementary assays—xCELLigence for cell viability, TUNEL for DNA fragmentation, and ATP level measurement—were employed to assess phototoxicity and its possible implications for surfactant-related processes.

For the xCELLigence analysis, cells were seeded at a density of $10^4$ cells per milliliter in specialized e-plates and cultured for 24 h. At this point, PBMT was administered at the predetermined energy density, including suboptimal and supramaximal levels. A control group was maintained without PBMT to provide baseline readings. Following exposure, the xCELLigence system monitored cell viability over 72 h, and the RTCA software (RTCA Software v.2.0, Roche) applied a sigmoidal dose-response equation to detect potential phototoxic effects. Cell index ratios for the treated groups were compared to the control group, with each experimental condition performed in triplicate.

DNA damage was evaluated using the TUNEL assay, a key indicator of genotoxicity. Cells were seeded at $10^4$ cells per milliliter in 24-well plates and exposed to the same PBMT energy density after 24 h of initial culture. The control group again remained untreated. Seventy-two hours

post-exposure, cells were harvested by trypsinization and examined using the Apo-Direct kit (BD Biosciences), which labels fragmented DNA. The resulting samples were analyzed on an Accuri C6 flow cytometer, and DNA fragmentation levels were quantified with the BD Accuri C6 software v.2.5. Each PBMT condition was conducted in triplicate. Genotoxicity was deemed absent when the PBMT-induced DNA fragmentation level was 20% or lower relative to the control group.

Because surfactant expression in lung type 2 alveolar epithelial cells is tightly correlated with cellular energy status, ATP content was quantified as an additional parameter. Cells were plated in 96-well plates at $10^4$ cells per milliliter and cultured for 24 h before being exposed to the same suboptimal, optimal, and supramaximal PBMT regimens. A control group was once more included. After 72 h, ATP levels were measured using the CellTiter-Glo Luminescent Cell Viability Assay (Promega), in accordance with the manufacturer's instructions. The luminescence was recorded on a Thermo Varioskan multi-plate reader, and each experimental condition was assessed in triplicate. To establish the relationship between ATP content and surfactant production, ATP measurements in the treatment groups were normalized to control values and subjected to correlation analysis. This comprehensive set of assays provided a robust framework for determining the safety and potential mechanistic effects of PBMT on human type 2 alveolar epithelial cells, thereby informing subsequent in vivo applications and optimizing treatment parameters.

## 2.6 Histochemical and immunohistochemical evaluation of premature rat lungs

Following euthanasia of the experimental animals, skin samples from the chest wall and premature lung tissues were rapidly collected to investigate potential structural and surfactant-related changes. These specimens were placed in 4% buffered formaldehyde solution for formalin-fixed, paraffin-embedded (FFPE) processing, remaining at room temperature for 24 h. Next, five-micron-thick sections were obtained using a Leica RM 2145 microtome. Each section was carefully floated on a 37 °C water bath to facilitate even spreading and subsequently mounted onto poly-L-lysine-coated slides. For deparaffinization, the sections were first incubated in xylene at 60 °C for one hour, followed by rehydration through a graded ethanol series (100% to 70%) for five minutes at each concentration.

For histochemical evaluation, two distinct staining protocols were employed. Routine Hematoxylin-Eosin (H ve E) staining was performed to visualize general tissue architecture, cellular morphology, and inflammatory changes. In addition, Masson's Trichrome stain (BioOptica Masson Trichrome with aniline blue, 04-010802, Milano, Italy) was used to highlight connective tissue components, thereby enabling a more detailed assessment of collagen distribution within the lung parenchyma. After staining, the slides were dehydrated in graded ethanol solutions, subjected to a 30-minute xylene treatment, and permanently mounted with Entellan to preserve the tissue for microscopic analysis.

Immunohistochemical staining was undertaken to elucidate the distribution and intensity of surfactant proteins (SP-A, SP-B, SP-C, and SP-D) in the premature lung tissue. These proteins serve critical functions in modulating surface tension and are composed predominantly of lipids. SP-A and SP-D, large hydrophilic proteins belonging to the collectin family of C-type lectins, play significant roles in immune defense, while SP-B and SP-C are smaller hydrophobic proteins vital for lowering alveolar surface tension. Sections were deparaffinized, treated with the appropriate antigen retrieval protocols as recommended for each antibody, and then incubated with specific primary antibodies targeting SP-A, SP-B, SP-C, or SP-D. Following secondary antibody application, detection was facilitated by a chromogenic substrate, and the tissues were counterstained and mounted with Entellan to allow detailed visualization under the microscope.

Microscopic evaluations were performed using an Olympus BX51 light microscope coupled with an Olympus DP72 camera for image capture. Forty measurements of the interalveolar septum thickness were recorded from distinct photomicrographs acquired at 40× magnification in each experimental group. Immunoreactivity was assessed semi-quantitatively using a standard scoring system based on staining intensity, ranging from 0 (no staining) to 3+ (strong immunoreactivity). Two independent histologists, blinded to the experimental groups, examined 40 photomicrographs from each group to minimize observer bias. This multi-faceted approach, combining histochemical and immunohistochemical techniques, provided comprehensive insights into lung structural integrity and surfactant protein expression patterns in premature rat lungs.

## 2.7 Statistical analysis

All statistical analyses were performed using GraphPad Prism v.10 (GraphPad Software). Data normality was assessed using the Shapiro-Wilk test. Continuous variables were expressed as mean ± standard deviation (SD). Group comparisons were conducted using one-way analysis of variance (ANOVA) followed by Tukey's post hoc test for parametric data, and the Kruskal-Wallis test followed by Dunn's multiple comparison test for non-parametric data. The correlation between surfactant protein levels, alveolar septal thickness, and physiological parameters was

evaluated using Pearson correlation coefficients, depending on data normality. Statistical significance was set at $p<0.05$.

## 3 Results

### 3.1 Physiological measurements

The study was conducted on 31 rat pups divided into six groups: 660 nm (LED/laser), 830 nm (LED/laser), and control (premature/mature) groups (Table 2). Body weight, temperature, oxygen saturation, heart rate, and respiratory rate were measured twice for all groups on day 0 and day 5. The descriptive statistics for these variables are presented in Table 5. There was a significant increase in body weight ($p<0.001$) and heart rate ($p=0.012$) across all groups (Table 6). Comparisons between experimental and control groups revealed no significant differences between the premature 660 nm/830 nm LED/laser groups and the premature control group, except for body weight. Oxygen saturation, heart rate, and respiratory rate measurements were obtained from the pelvic region using a Covidien device; however, due to mechanical irritations during measurements, expected differences among these variables were not observed. Furthermore, no significant increase in surface temperature related to light penetration was detected.

**Table 5** Descriptive statistics table of physiological data collected from the groups

| Descriptive statistics | | | | | |
|---|---|---|---|---|---|
| | N | Minimum | Maximum | Mean | Std. deviation |
| Weight1 (g) | 31 | 6 | 12 | 8.19 | 1.815 |
| Weight2 (g) | 31 | 8 | 20 | 12.19 | 3.842 |
| Temperature1 (°C) | 31 | 26 | 60 | 36.67 | 4.662 |
| Temperature2 (°C) | 31 | 36 | 38 | 36.08 | 0.426 |
| Oxygen sat1 (%) | 31 | 58 | 86 | 75.45 | 7.289 |
| Oxygen sat2 (%) | 31 | 47 | 96 | 73.35 | 11.185 |
| Heart beat1 (bpm- beats per minute) | 31 | 104 | 179 | 131.23 | 21.307 |
| Heart beat2 (bpm- beats per minute) | 31 | 97 | 196 | 144.94 | 23.859 |
| Respiratory rate1 (breaths per minute- bpm) | 31 | 9 | 25 | 15.68 | 3.763 |
| Respiratory rate2(breaths per minute- bpm) | 31 | 7 | 23 | 14.90 | 3.902 |
| Valid N (listwise) | 31 | | | | |

### 3.2 Surfactant protein quantification

The application of 660 nm PBMT on premature rat lungs resulted in an increase in surfactant proteins, although the increase in surfactant A was not significant for either LED ($p=0.9992$) or laser ($p=0.5151$) treatments (Fig. 3).

Significant increases were observed for surfactant B (LED: $p=0.0255$, laser: $p=0.0189$), surfactant C (LED: $p=0.0206$, laser: $p=0.0005$), and surfactant D (LED: $p=0.0001$, laser: $p<0.0001$) (Figs. 4, 5 and 6). However, 830 nm PBMT did not show a significant increase in surfactant levels. For the 830 nm treatment, no significant increases were observed in surfactant A (LED: $p=0.9981$, laser: $p=0.2382$), B (LED: $p=0.0998$, laser: $p=0.7530$), or C (LED: $p=0.6339$, laser: $p=0.2013$). In surfactant D, no significant increase was detected in the laser group ($p=0.1350$), but a significant increase was found in the LED group ($p=0.0388$, Fig. 7).

### 3.3 Phototoxicity and cellular responses in alveolar cells

#### 3.3.1 Cell viability

No phototoxic effects were observed on type 2 alveolar cells at 660 nm and 30 mW at 1, 3, and 5 J/cm² energy densities. At 24 h, significant increases in cell viability were detected at 1 ($p=0.0448$), 3 ($p=0.0037$), and 5 J/cm² ($p=0.0179$) compared to controls. At 48 h, significant increases were noted at 3 ($p=0.0475$) and 5 J/cm² ($p=0.0162$), though the 1 J/cm² energy density showed no significance. At 72 h, all three energy densities exhibited significant increases in viability. The 3 J/cm² energy density demonstrated high significance across all time points.

#### 3.3.2 DNA fragmentation analysis

No apoptotic DNA fragmentation was detected, suggesting that PBM did not induce apoptosis in alveolar cells.

#### 3.3.3 ATP level assessment

PBMT at 3 J/cm², as well as lower and higher energy densities, did not show ATP level increases. However, ATP might have been consumed for surfactant production and cellular activities, explaining the lack of an observable increase. The absence of ATP depletion and the observed increase in cell viability support this conclusion.

**Table 6** Paired samples test table for physiological data before and after PBMT treatment

Paired samples statistics

| | | Mean | N | Std. deviation | Std. error mean |
|---|---|---|---|---|---|
| Pair 1 | Weight1 (g) | 8.19 | 31 | 1.815 | 0.326 |
| | Weight2 (g) | 12.19 | 31 | 3.842 | 0.690 |
| Pair 2 | BodyTemp1 (°C) | 36.67 | 31 | 4.662 | 0.837 |
| | BodyTemp2 (°C) | 36.08 | 31 | 0.426 | 0.077 |
| Pair 3 | SPO1 (%) | 75.45 | 31 | 7.289 | 1.309 |
| | SPO2 (%) | 73.35 | 31 | 11.185 | 2.009 |
| Pair 4 | HeartRate1 (bpm - beats per minute) | 131.23 | 31 | 21.307 | 3.827 |
| | HeartRate2(bpm- beats per minute) | 144.94 | 31 | 23.859 | 4.285 |
| Pair 5 | RespRate1 (breaths per minute- bpm) | 15.68 | 31 | 3.763 | 0.676 |
| | RespRate2 (breaths per minute- bpm) | 14.90 | 31 | 3.902 | 0.701 |

Paired samples test

| | | Paired differences 95% confidence interval of the difference | | | | | t | df | Sig. (2-tailed) |
|---|---|---|---|---|---|---|---|---|---|
| | | Mean | Std. deviation | Std. error mean | Lower | Upper | | | |
| Pair 1 | Weight1 (g) Weight2 (g) | -4.000 | 2.530 | 0.454 | -4.928 | -3.072 | -8.803 | 30 | 0.000 |
| Pair 2 | BodyTemp1 BodyTemp2 (°C) | 0.590 | 4.746 | 0.852 | -1.151 | 2.331 | 0.693 | 30 | 0.494 |
| Pair 3 | SPO1 (%) SPO2 (%) | 2.097 | 13.712 | 2.463 | -2.933 | 7.126 | 0.851 | 30 | 0.401 |
| Pair 4 | HeartRate1 HeartRate2 (bpm- beats per minute) | -13,710 | 28.527 | 5.124 | -24.174 | -3.246 | -2.676 | 30 | 0.012 |
| Pair 5 | RespRate1 RespRate2 (breaths per minute- bpm) | 0.774 | 4.863 | 0.873 | -1.010 | 2.558 | 0.886 | 30 | 0.382 |

## 3.4 Histopathological examination

### 3.4.1 Chest wall histology

Histological examination of chest wall skin samples in the control group revealed intact epidermal stratification, well-preserved hair follicles and sebaceous glands, and normal collagen structure. Masson's Trichrome staining confirmed consistent connective tissue content. Experimental groups showed histology comparable to controls, with no significant histopathological changes observed (Fig. 8). Neither 660–830 nm LED or laser treatments caused histopathological damage to the chest wall.

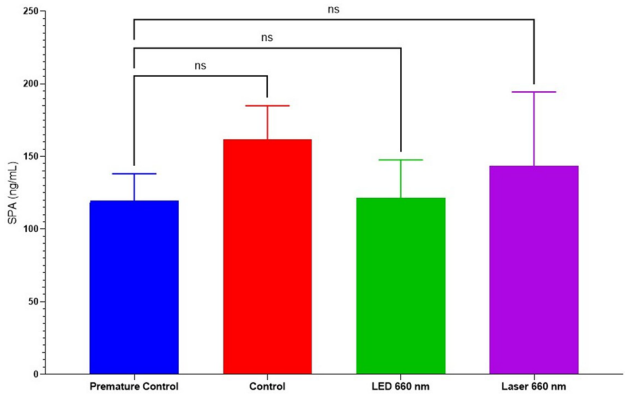


| Dunnett's multiple comparisons test | Summary | Adjusted P Value |
|---|---|---|
| Premature Control vs. Control | ns | 0.2335 |
| Premature Control vs. LED 660 nm | ns | 0.9992 |
| Premature Control vs. Laser 660 nm | ns | 0.5151 |

**Fig. 3** Statistical graphs of surfactant A increase following 660 nm PBMT

### 3.4.2 Lung parenchymal analysis

Examination of the lung parenchyma in the control group showed normal alveolar ducts, terminal bronchioles, and alveoli. As lung development in rats continues in the saccular stage until postnatal day 5, less septalization and thicker interalveolar septa were observed compared to adult lungs. In the 660 nm LED, 660 nm laser, and 830 nm LED groups, interalveolar septa were slightly thickened compared to controls. Only the 830 nm laser group exhibited the greatest septal thickness and occasional erythrocyte extravasation. Masson's Trichrome staining indicated consistent connective tissue content across all groups (Fig. 9).

### 3.4.3 Immunohistochemical evaluation of surfactant proteins

SP-A immunoreactivity was highest in the 830 nm LED and 830 nm laser groups, whereas lower immunoreactivity was observed in the 660 nm LED, 660 nm laser, and control

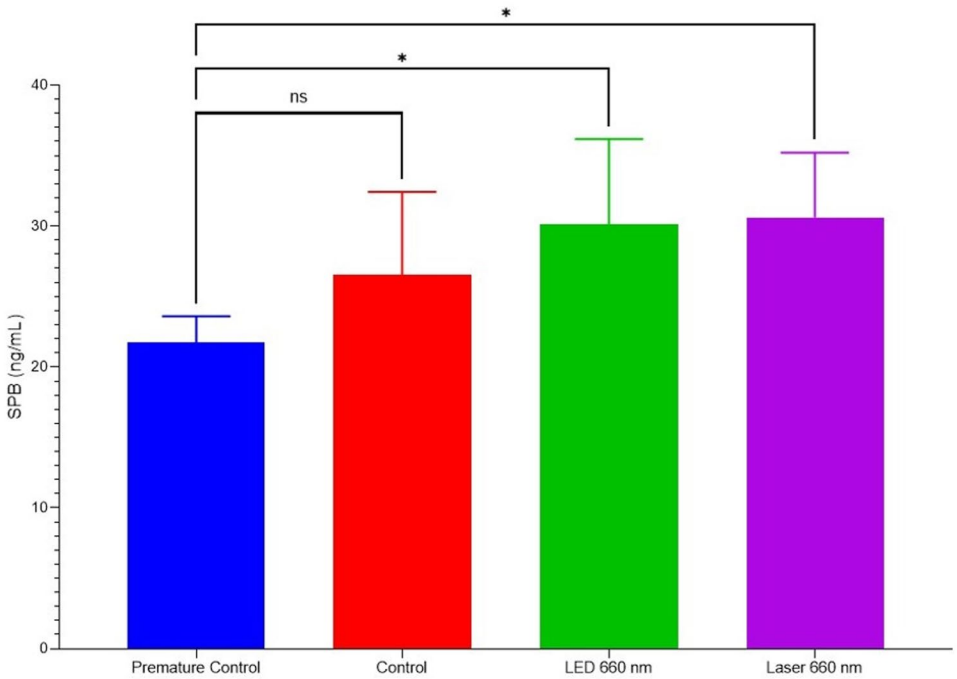


**Fig. 4** Statistical graphs of surfactant B increase following 660 nm PBMT

| Dunnett's multiple comparisons test | Summary | Adjusted P Value |
|---|---|---|
| Premature Control vs. Control | ns | 0.3978 |
| Premature Control vs. LED 660 nm | * | 0.0255 |
| Premature Control vs. Laser 660 nm | * | 0.0189 |

groups. SP-B immunoreactivity was low across all groups, with no significant differences detected. SP-C immunoreactivity was high in the 830 nm LED and 830 nm laser groups, moderate in the 660 nm LED and 660 nm laser groups, and lowest in the control group. SP-D immunoreactivity was moderate to high in the 830 nm LED, 660 nm laser, and 830 nm laser groups, while lower immunoreactivity was noted in the control and 660 nm LED groups. The 830 nm wavelength generally produced higher immunoreactivity across surfactant proteins compared to 660 nm. The LED and laser applications demonstrated similar immunoreactivity trends, with slight variations in intensity. Among surfactant proteins, SP-C and SP-D exhibited the most prominent immunoreactivity in PBMT groups. The control group consistently showed the lowest immunoreactivity for all surfactant proteins. Immunohistochemical staining indicated that PBMT may influence surfactant protein expression. The findings suggest that 830 nm PBMT has a more pronounced effect on surfactant proteins compared to 660 nm. These results highlight potential benefits of PBMT in surfactant protein regulation. The observed immunoreactivity patterns indicate the potential of PBMT for modulating lung surfactant production (Fig. 10).

## 4 Discussion

Surfactants are critical surface-active agents necessary for normal lung function and are utilized therapeutically in cases of respiratory tract injury or infection. Their production and secretion are dependent on the metabolic activity of respiratory epithelial cells. Consequently, infrared PBMT may enhance surfactant synthesis by stimulating the metabolic processes of these cells.

Our findings align with the study objectives and demonstrate a positive impact of PBMT on surfactant production. In conventional invasive surfactant therapies, preparations typically include only Surfactant B and C proteins, whereas Surfactant A and D proteins are absent. In our experimental model, PBMT applied to rat lungs resulted in a significant increase in Surfactant B, C, and D proteins, with no significant change observed in Surfactant A levels (Fig. 3). Specifically, application of 660 nm LED and laser

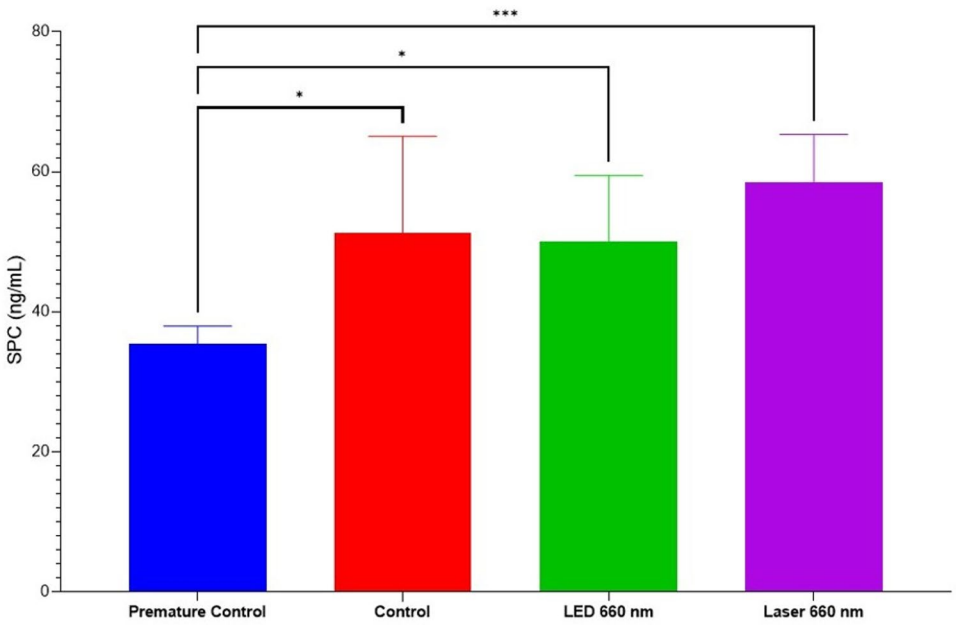


**Fig. 5** Statistical graphs of surfactant C increase following 660 nm PBMT

| Dunnett's multiple comparisons test | Summary | Adjusted P Value |
|---|---|---|
| Premature Control vs. Control | * | 0.0395 |
| Premature Control vs. LED 660 nm | * | 0.0206 |
| Premature Control vs. Laser 660 nm | *** | 0.0004 |

treatments—administered three times daily for three days at 3 J/cm² energy density and 30 mW nominal power—significantly elevated surfactant levels (Figs. 4, 5 and 6). The 660 nm wavelength alone was insufficient to stimulate the synthesis of Surfactant A.

To our knowledge, no previous studies have directly compared the effects of infrared PBMT on surfactant levels, particularly in preterm rat models of RDS. Thus, this study is the first to investigate surfactant modulation via infrared PBMT in a model relevant to premature newborns with RDS.

Light therapy, known as PBM or Low-Level Laser Therapy (LLLT), demonstrates a broad therapeutic potential owing to its anti-inflammatory and tissue-reparative properties. In the literature, the positive effects of PBMT on fundamental biological processes such as promoting cell proliferation, accelerating wound healing, increasing collagen production, and reducing inflammation have also been emphasized by Prindeze et al. [12]. These effects explain the therapy's efficacy in reducing pain, inflammation, and edema, and they indicate its potential for even more severe conditions in the future, such as stroke, myocardial infarction, and degenerative brain diseases [13].

The symptoms of ARDS and severe pulmonary inflammation, the significance of which has been further highlighted by the COVID-19 pandemic, can be managed with PBMT. It has been concluded that, when applied in the early stages of the disease, PBM is a promising and cost-effective method that can reduce life-threatening complications by increasing oxygenation and modulating inflammation [14, 15]. A systematic review by Nejatifard et al. concluded that PBMT, particularly using infrared lasers or LEDs that can penetrate deeper tissues, could be a promising adjunctive treatment for reducing COVID-19-related pulmonary inflammation, repairing tissue damage, and improving the patient's overall condition [9]. Supporting these findings, an animal study by Lima et al. demonstrated that 660 nm LLLT could effectively control pulmonary inflammation resulting from systemic injury by suppressing pro-inflammatory mediators and triggering anti-inflammatory responses in a dose-dependent manner [16]. Furthermore, the study by Cury et al. drew attention not only to the efficacy of this treatment but also to its safety, revealing that 660 nm LLLT reduces acute pulmonary inflammation without impairing lung function or increasing the long-term risk of fibrosis [17]. These preclinical and review findings are

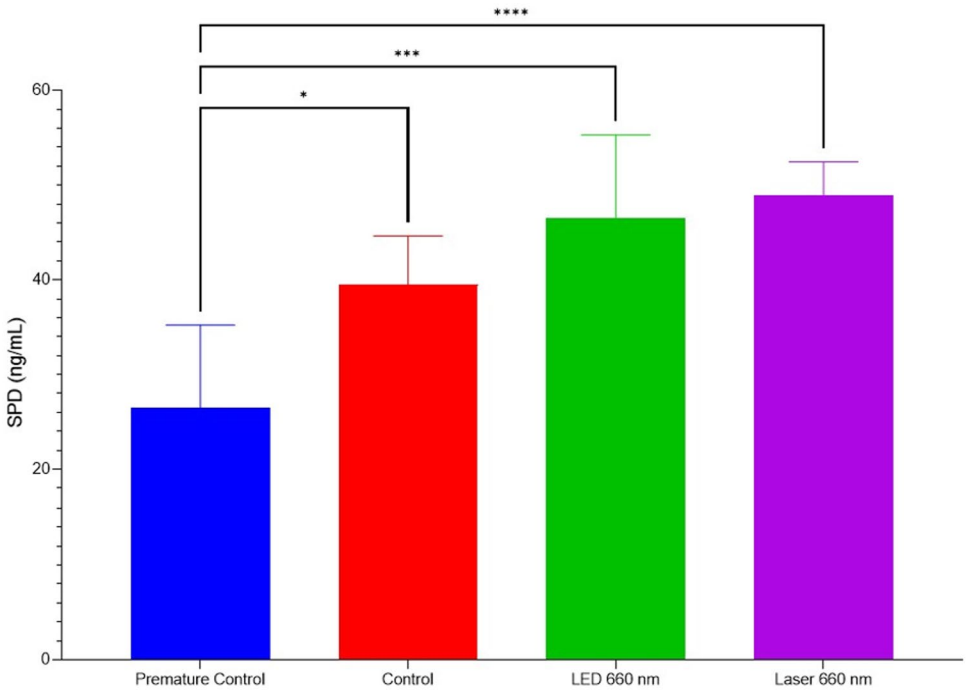


**Fig. 6** Statistical graphs of surfactant D increase following 660 nm PBMT

| Dunnett's multiple comparisons test | Summary | Adjusted P Value |
|---|---|---|
| Premature Control vs. Control | * | 0.0330 |
| Premature Control vs. LED 660 nm | *** | 0.0001 |
| Premature Control vs. Laser 660 nm | **** | <0.0001 |

also corroborated at the clinical level by a case report showing that PBM therapy in two patients with acute respiratory syndrome symptoms reduced life-threatening complications by improving oxygenation and modulating inflammation.

The reparative and anti-inflammatory effects of PBMT are not limited to pulmonary tissue; they have also been proven in wound healing, one of the therapy's most well-known applications. Min and Goo reported that 830 nm LED-LLLT accelerated healing in wounds of various etiologies, controlled secondary infections, and was a painless method well-tolerated by patients [18]. Similarly, Yadav and Gupta stated that PBMT offers a non-invasive and painless alternative, especially for chronic skin wounds where conventional treatments have failed [19]. The potential of PBMT therapy extends beyond these applications to more complex areas such as neurodegenerative diseases. A study by Reinhart et al. in a Parkinson's disease model proved that 810 nm near-infrared (NIR) light therapy exhibited both neuroprotective effects and improved motor skills. This study is significant as it demonstrates that deeper-penetrating wavelengths, such as 810 nm, may be superior for symptomatic recovery compared to the previously studied 670 nm. The existing literature strongly supports that PBMT/LLLT can offer therapeutic benefits in a wide variety of pathological conditions by acting through fundamental cellular mechanisms. The efficacy demonstrated across a broad spectrum—from acute lung injury to chronic wounds and neurodegenerative models—underscores the future clinical potential of this non-invasive and safe treatment method [20, 21].

There are no studies in the literature investigating an increase in surfactant using PBMT. Kassab et al. (2022) reported in their study that photodynamic therapy using an 808 nm laser and a 660 nm LED may have potential as a successful treatment for pneumonia [22]. This study does not examine the effects of PBMT on surfactant increase.

The study of Özdemir et al. (2025) is the first to examine the increase in pulmonary surfactant through the application of PBMT. In this work, the use of 660 nm light not only significantly increased surfactant levels but did so without detectable cellular or tissue phototoxicity. Overall, 660 nm

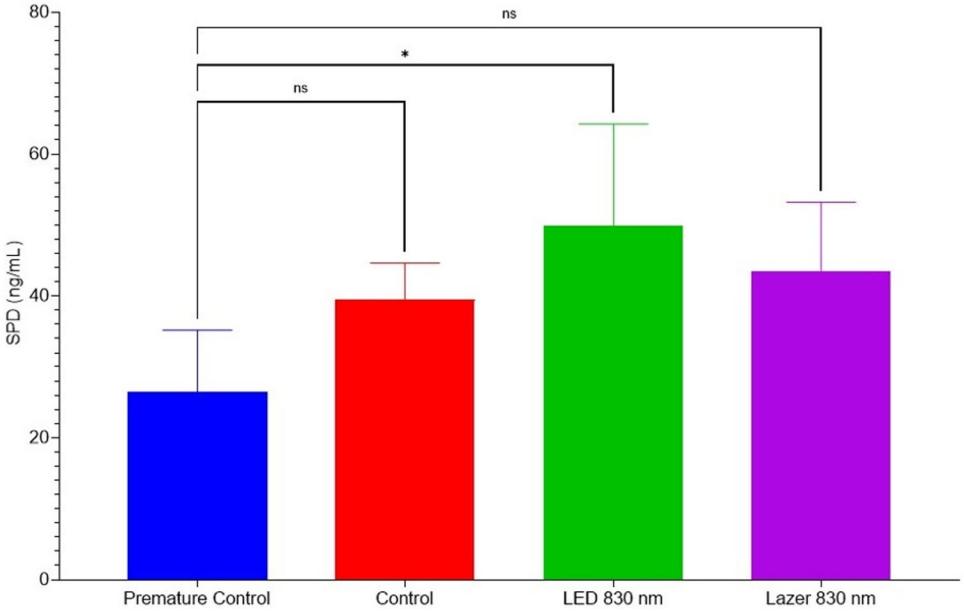


**Fig. 7** Statistical graphs of surfactant D increase following 830 nm PBMT

| Dunnett's multiple comparisons test | Summary | Adjusted P Value |
|---|---|---|
| Premature Control vs. Control | ns | 0.1669 |
| Premature Control vs. LED 830 nm | * | 0.0388 |
| Premature Control vs. Lazer 830 nm | ns | 0.1350 |

infrared PBMT —administered at 30 mW power, 3 J/cm² energy, three times daily for three days—led to significant increases in Surfactant B, C, and D in premature rat lungs compared to controls, with a modest, non-significant rise in Surfactant A. Our histological and cytotoxic assessments revealed no significant tissue or cellular damage. Furthermore, the increased interalveolar septal thickness observed in the 660 nm LED and laser groups suggests an enhancement in lung alveolar development. In contrast, although 830 nm LED and laser applications led to increases in some surfactant proteins, they were accompanied by decreased cell viability, erythrocyte extravasation, and heightened immune reactivity, which are indicative of adverse outcomes.

These findings suggest that 660 nm infrared PBMT may offer a significant therapeutic advantage in the management of both neonatal RDS and adult ARDS. We believe that this method, which we have developed, could serve as a standalone and/or adjunctive treatment modality and that its application could potentially improve clinical outcomes.

Conventional surfactant applications, whether using natural or synthetic preparations, are invasive procedures. Complications related to the administration route and the surfactant itself can also arise, prolonging the hospital stay for infants in intensive care. This situation increases healthcare costs and brings social and physiological trauma to the family and the newborn. To overcome these aforementioned problems and to develop a new non-invasive treatment method, we believe that the infrared PBM method would be suitable for the treatment of neonatal RDS. It is anticipated that this non-invasive method could eliminate complications associated with currently used invasive methods and thereby reduce the burden on the healthcare economy. Further clinical studies in both infants and adults are required to explore the translational potential of these preclinical findings. Additionally, all adult pneumonias, including COVID-19 pneumonia, a global pandemic, damage alveolar type I and type II surfactant-producing cells. Decreased surfactant production also contributes to the development of ARDS. The aforementioned problems in treating premature infants with RDS are also significant for adults. It is thought that the PBM device we have developed will be a non-invasive alternative treatment method to conventional invasive approaches for both infants with RDS and adults suffering from ARDS.

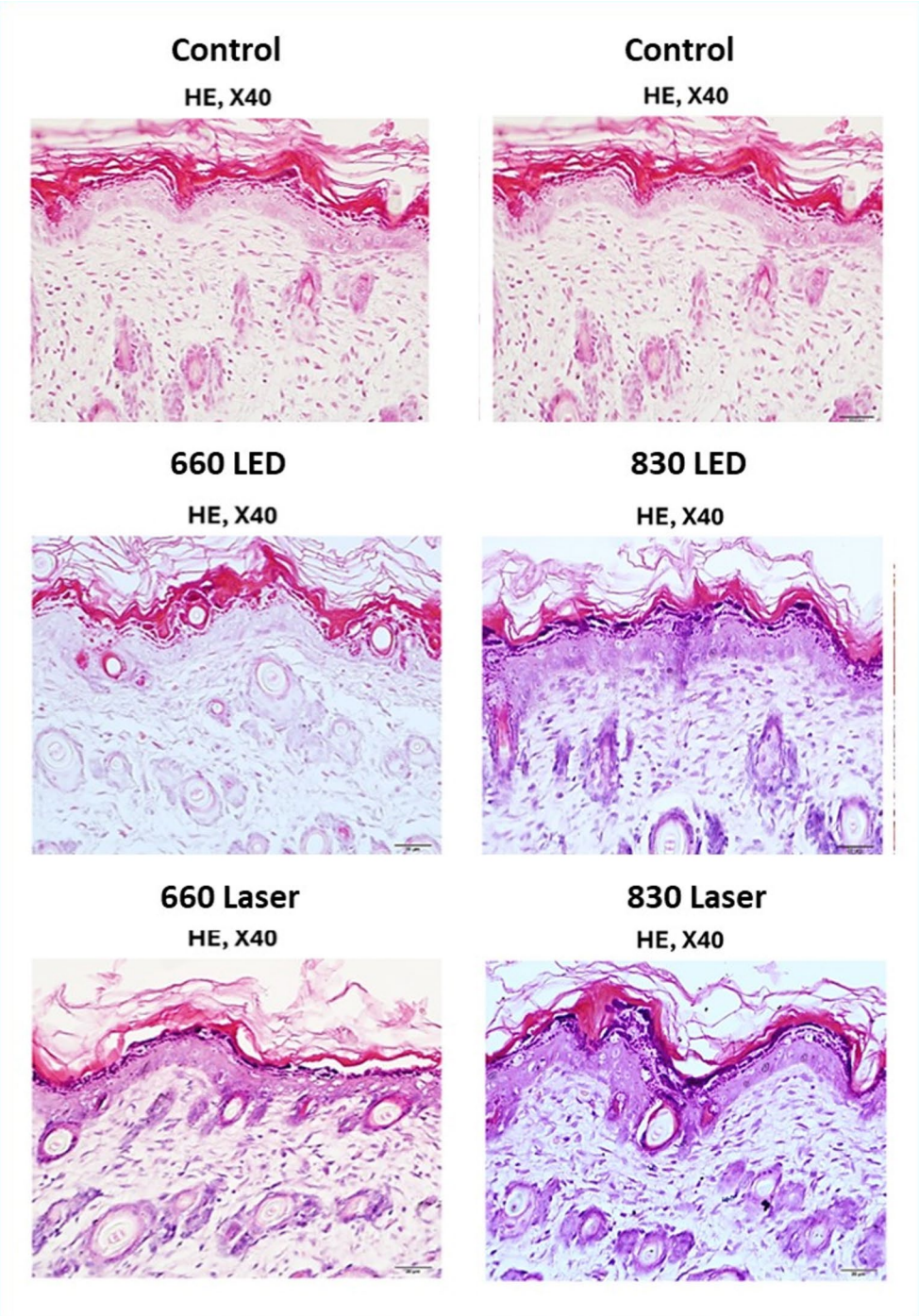


**Fig. 8** Histological examination of chest wall skin samples. *HE* Hematoxylin ve Eosin. *MT* Masson's Trichrome

## 5 Conclusion

The findings of this study demonstrate that PBMT administered at a 660 nm wavelength (LED or laser), 30 mW power, and 3 J/cm² energy—applied over 375 s for LED and 234 s for laser, three times per day for three consecutive days—effectively increased surfactant levels in the lungs of premature rat pups. Notably, no cytotoxic or phototoxic damage was detected in lung cells or tissues. These results underscore the potential of 660 nm PBMT as an adjunct or alternative therapy for premature infants with RDS and adults with ARDS, warranting further clinical investigation.

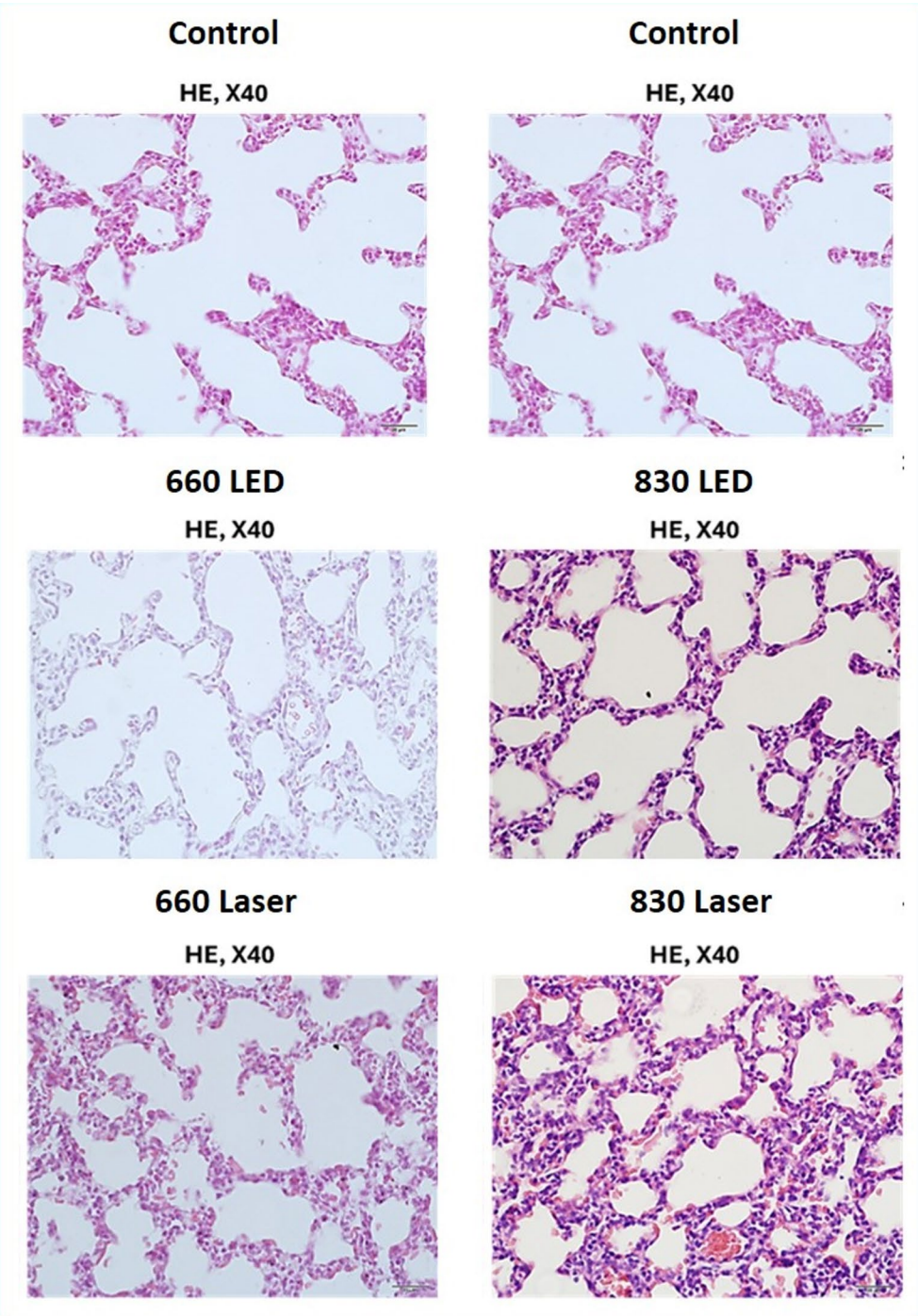


**Fig. 9** Photomicrographs of histological examination of lung tissues. *HE* Hematoxylin ve Eosin. *MT* Masson's Trichrome

## 5.1 Limitations of our study

A primary limitation of this study involved the considerable difficulty in maintaining the viability of premature rat pups, particularly those obtained on gestational day 18, which could not be kept alive. Even pups obtained on days 19–20 experienced survival challenges. Additionally, oxygen saturation and heart rate measurements were restricted to the pelvic region, necessitating mechanical manipulation that may have adversely influenced the accuracy of these measurements. These factors likely impacted the reliability and interpretability of the physiological data obtained.

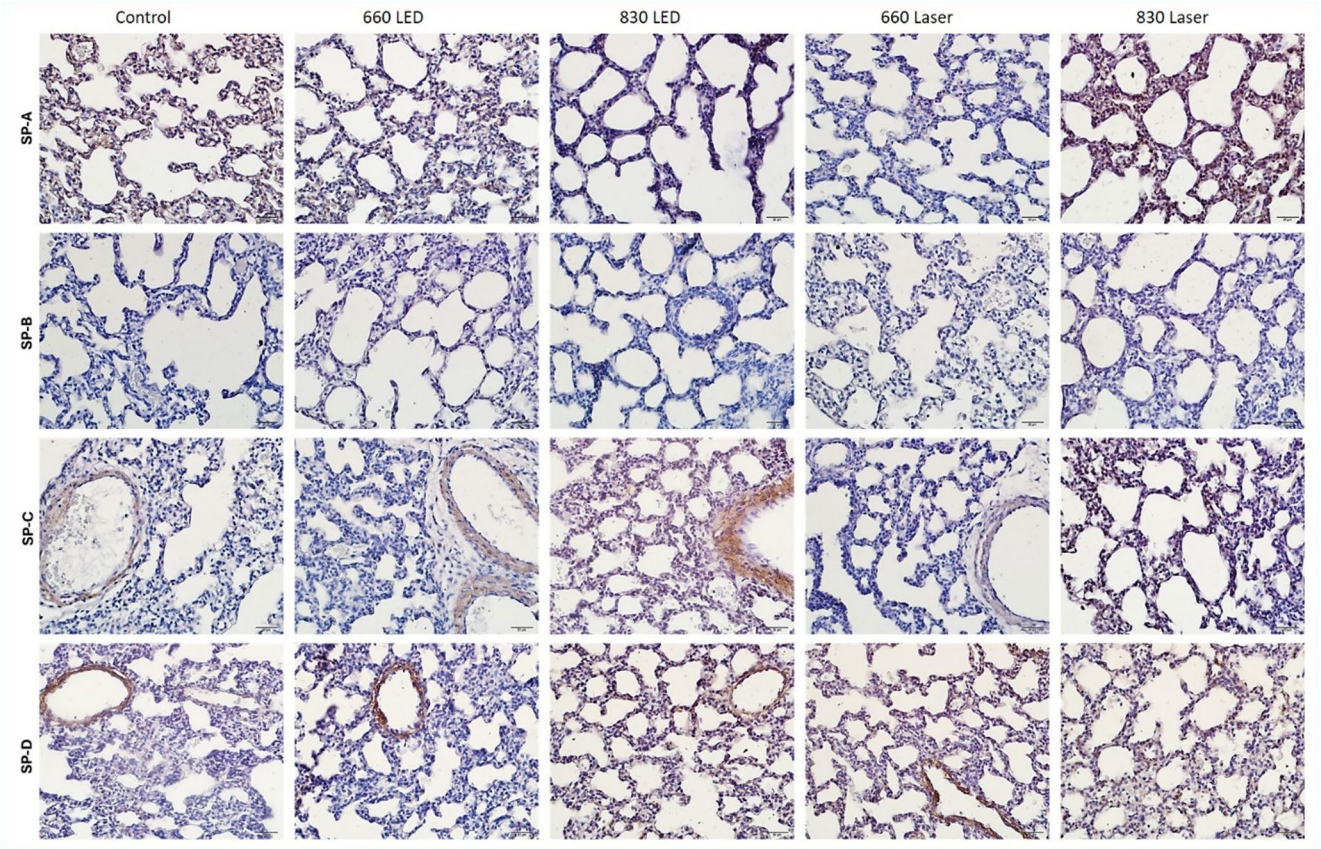


**Fig. 10** Photomicrographs of immunohistochemical examination of lung tissues, x40 magnification

**Supplementary Information** The online version contains supplementary material available at https://doi.org/10.1007/s43630-025-00820-w.

**Acknowledgements** This study (Project no SBAG 221S431) received both scientific and financial support from The Scientific and Technological Research Council of Turkey (TÜBİTAK). The authors gratefully acknowledge this contribution, which was instrumental in facilitating the research described herein. Patent applications for this device have been filed under national patent number 2023/019371 and international patent number PCT/TR2024/051826.

**Author contributions** All authors contributed equally to the research and the prepared publication.

**Funding** None. The authors declared that this study has received no financial support.

**Data availability** The data that support the findings of this study are available from the corresponding author upon reasonable request.

## Declarations

**Conflict of interest** The authors declare no competing interests.

**Informed consent** This study was approved by the Local Animal Experiments Ethics Committee of Ege University (Protocol No: 2021-077, dated 29.09.2021). No human participants were involved.

## References

1. Weaver, T. E., & Conkright, J. J. (2001). Function of surfactant proteins B and C. *Annual Reveiw of Physiology*, *63*, 555–78PMID: 11181967.
2. Fehrenbach, H. (2001). Alveolar epithelial type II cell: Defender of the alveolus revisited. *Respiratory Research*, *2*(1), 33–46. https://doi.org/10.1186/rr36Epub 2001 Jan 15. PMID: 11686863; PMCID: PMC59567.
3. Matthay, M. A., Zemans, R. L., Zimmerman, G. A., Arabi, Y. M., Beitler, J. R., et al. (2019). Acute respiratory distress syndrome. *Nature Reviews Disease Primers*, *5*(1), 18. https://doi.org/10.1038/s41572-019-0069-0PMID: 30872586; PMCID: PMC6709677.
4. Hamblin, M. R., & Demidova, T. N. (2006). Mechanisms of low-level light therapy. *SPIE*. https://doi.org/10.1117/12.646294
5. Freitas, L. F., & Hamblin, M. R. (2016). Proposed mechanisms of photobiomodulation or low-level light therapy. *IEEE Journal of Selected Topics in Quantum Electronics*, *22*(3), 7000417. https://doi.org/10.1109/JSTQE.2016.2561201PMID: 28070154; PMCID: PMC5215870.
6. Lima, F. M., Albertini, R., Dantas, Y., Maia-Filho, A. L., de Loura Santana, C., Castro-Faria-Neto, H. C., França, C., Villaverde, A. B., & Aimbire, F. (2013). Low-level laser therapy restores the oxidative stress balance in acute lung injury induced by gut ischemia and reperfusion. *Photochemistry and Photobiology*, *89*(1), 179–188. https://doi.org/10.1111/j.1751-1097.2012.01214.xEpub 2012 Nov 19. PMID: 22882462.
7. Torres-Silva, R., Lopes-Martins, R. A., Bjordal, J. M., Frigo, L., & Rahouadj, R. (2015). The low level laser therapy (LLLT) operating in 660 Nm reduce gene expression of inflammatory

mediators in the experimental model of collagenase-induced rat tendinitis. *Lasers in Medical Science*, *30*(7), 1985–1990. https://doi.org/10.1007/s10103-014-1676-3Epub 2014 Nov 8. PMID: 25380666.
8. Brochetti, R. A., Leal, M. P., Rodrigues, R., da Palma, R. K., & de Oliveira, L. V. F., et al. (2017). Photobiomodulation therapy improves both inflammatory and fibrotic parameters in experimental model of lung fibrosis in mice. *Lasers in Medical Science*, *32*(8), 1825–1834. https://doi.org/10.1007/s10103-017-2281-z.Epub 2017 Jul 16. PMID: 28712048.
9. Nejatifard, M., Asefi, S., Jamali, R., Hamblin, M. R., & Fekrazad, R. (2021). Probable positive effects of the photobiomodulation as an adjunctive treatment in COVID-19: A systematic review. *Cytokine*, *137*, 155312. https://doi.org/10.1016/j.cyto.2020.155312Epub 2020 Oct 12. PMID: 33128927; PMCID: PMC7550078.
10. Özdemir, H. İ., Bilge, M., Özkan, E., Günel, N. S., Özdemir, H. E., Ahadova, A., Çekin, A., Çelebi, L. M. O., Kayabaşı, Ç., Çetinel, Z. Ö., Bilge, D., Koylu, M., Tomruk, C. Ş., Tomruk, C., Şanlıer, Ş., Terek, D., Erol, E., Soylu, F. E., Yalaz, M., Oran, İ., & Gündüz, C. (2025). Effect of photobiomodulation therapy on surfactant production increase in human lung epithelial alveolar cells. *Photochemical & Photobiological Sciences*, *24*(9), 1617–1632. https://doi.org/10.1007/s43630-025-00784-xEpub 2025 Sep 25. PMID: 40999280.
11. Jenkins, P. A., & Carroll, J. D. (2011). How to report low-level laser therapy (LLLT)/photomedicine dose and beam parameters in clinical and laboratory studies. *Photomedicine and Laser Surgery*, *29*(12), 785–787. https://doi.org/10.1089/pho.2011.9895
12. Prindeze, N. J., Moffatt, L. T., & Shupp, J. W. (2012). Mechanisms of action for light therapy: A review of molecular interactions. *Experimental Biology and Medicine*, *237*, 1241–1248. https://doi.org/10.1258/ebm.2012.012063
13. Farivar, S., Malekshahabi, T., & Shiari, R. (2014). Biological effects of low level laser therapy. *Journal of Lasers in Medical Sciences*, *5*, 58–62. https://doi.org/10.22037/jlms.v5i2.2370
14. Pelletier-Aouizerate, M., & Zivic, Y. (2021). Early cases of acute infectious respiratory syndrome treated with photobiomodulation, diagnosis and intervention: Two case reports. *Clinical Case Reports*, *9*, 2429–2437. https://doi.org/10.1002/ccr3.4000
15. Isasi-Campillo, M., Losada-Oliva, P., Pérez-Gil, J., Olmeda, B., & García-Ortega, L. (2023). Pulmonary surfactant-derived antiviral actions at the respiratory surface. *Current Opinion in Colloid Ve Interface Science*, *66*, 101711. https://doi.org/10.1016/j.cocis.2023.101711
16. Lima, F. M., Aimbire, F., Miranda, H., Vieira, R. P., & de Oliveira, A. P. (2014). Low-level laser therapy attenuates the myeloperoxidase activity and inflammatory mediator generation in lung inflammation induced by gut ischemia and reperfusion: A dose-response study. *Journal of Lasers in Medical Sciences*, *5*(2), 63–70. https://doi.org/10.22037/jlms.v5i2.2371
17. Cury, V., de Lima, T. M., Prado, C. M., Pinheiro, N., Ariga, S. K., et al. (2016). Low level laser therapy reduces acute lung inflammation without impairing lung function. *Journal of Biophotonics*, *9*, 1199–1207. https://doi.org/10.1002/jbio.201500278
18. Min, P. K., & Goo, B. L. (2013). 830 Nm light-emitting diode low level light therapy (LED-LLLT) enhances wound healing: A preliminary study. *Laser Therapy*, *22*, 43–49. https://doi.org/10.5978/islsm.13-OR-07
19. Yadav, A., & Gupta, A. (2017). Noninvasive red and near-infrared wavelength-induced photobiomodulation: Promoting impaired cutaneous wound healing. *Photodermatology Photoimmunology ve Photomedicine*, *33*(1), 4–13. https://doi.org/10.1111/phpp.12228
20. Reinhart, F., Massri, N. E., Darlot, F., Torres, N., Johnstone, D. M., et al. (2015). 810 Nm near-infrared light offers neuroprotection and improves locomotor activity in MPTP-treated mice. *Neuroscience Research*, *92*, 86–90. https://doi.org/10.1016/j.neures.2014.12.001
21. Reinhart, F., Massri, N. E., Torres, N., Chabrol, C., Molet, J., et al. (2017). The behavioural and neuroprotective outcomes when 670 Nm and 810 Nm near infrared light are applied together in MPTP-treated mice. *Neuroscience Research*, *117*, 42–47. https://doi.org/10.1016/j.neures.2016.12.005
22. Kassab, G., Diaz Tovar, J. S., Souza, L. M. P., Costa, R. K. M., Silva, R. S., Pimentel, A. S., Kurachi, C., & Bagnato, V. S. (2022). Lung surfactant negatively affects the photodynamic inactivation of bacteria-in vitro and molecular dynamic simulation analyses. *Proceedings of the National Academy of Sciences U S A*, *119*(25), e2123564119. https://doi.org/10.1073/pnas.2123564119Epub 2022 Jun 13. PMID: 35696565; PMCID: PMC9231493.